Talanta 84 (2011) 53–59

Contents lists available at ScienceDirect

Talanta

journal homepage: www.elsevier.com/locate/talanta

A hybrid mesoporous material functionalized by 1,8-naphthalimide-base receptor and the application as chemosensor and absorbent for Hg^{2+} in water

Qingtao Meng, Xiaolin Zhang, Cheng He, Peng Zhou, Weiping Su, Chunying Duan*

State Key Laboratory of Fine Chemicals, Dalian University of Technology, 158 Zhongshan Road, Dalian 116012, China

ARTICLE INFO

Article history:
Received 9 September 2010
Received in revised form
24 November 2010
Accepted 4 December 2010
Available online 13 December 2010

Keywords:
Fluorescence dye
Hg^{2+}
Silica material
Absorbent
Toxicide

ABSTRACT

A novel hybrid material (SBA-**P1**) is prepared through the functionalization of mesoporous silica (SBA-15) with a 1,8-naphthalimide-based dye by sol–gel reaction. The characterization results of elemental analysis (EA), X-ray powder diffractometer (XRD) and spectroscopic methods demonstrate the fluorescence dye **P1** is successfully grafted onto the inner surface of SBA-15 and the organized structure is preserved. SBA-**P1** can detect Hg^{2+} with high selectivity to Cu^{2+}, Zn^{2+}, Cd^{2+}, Pb^{2+}, Mn^{2+}, Ni^{2+}, Co^{2+}, Ag^{+}, Cr^{3+}, and Mg^{2+}, Ca^{2+}, Li^{+}, Na^{+}, K^{+} in water and sensitivity to environmentally relevant mercury in complex natural samples. The quenching fluorescence detection is also reversible by treating with EDTA/base. Furthermore, its fluorescence intensity keeps stable in the physiologically relevant pH range. The extraction ability of SBA-**P1** is also estimated by inductively coupled plasma source mass spectrometer (ICP), showing that approximately 90% of the Hg^{2+} ion is extracted. These results imply that the hybrid material has potential application for sensing and removing of Hg^{2+} ions in waste water and working as toxicide for acute mercury poisoning.

1. Introduction

Mercury is one of the most dangerous and ubiquitous of pollutants, and its contamination is widespread and arises from a variety of natural and anthropogenic sources [1,2]. Once mercury is introduced into the food chains as a result of bioaccumulation, this environmental cycle causes serious threat to the human health and ecology [3–5]. Accordingly, the development of new or improved analytical methods for sensing and removing of Hg^{2+}, applicable in a wide range of different sites and environments, is highly desirable [6–11]. Up to now, several types of small organic molecules [12–19], oligonucleotides [20], proteins [21], DNA and DNAzyme [22] platforms have been examined as Hg^{2+}-responsive groups in fluorescent chemosensors. However, their use in related analytical techniques in the homogeneous phase has not been appropriate for the separation, removal, and enrichment of target species.

Recently, organic–inorganic hybrid materials have received much attention due to their potential use in catalysis [23], optical devices [24–28] and drug delivery [29,30]. Receptors immobilized on inorganic nanomaterials have important advantages when used in the heterogeneous solid–liquid phase [31]. In particular, mesoporous silica (e.g., SBA-15 or MCM-41) appears to be more attractive as a promising inorganic support material due to its excellent properties [32]. Firstly, mesoporous silica materials themselves are nonfluorescent, but they possess high surface area with abundant hydroxyl groups on the pore walls that can act as binding sites for the covalent grafting of fluorophores on the silicon wall. Furthermore, the mesoporous silica materials are optical transparency in the visible region, which also makes such silica-based material particularly suitable for promising chemosensor substrates. Secondly, the ordered channel and larger pore size of mesoporous silica facilitate the lowering of diffusion resistance and enhancement of accessibility. Thirdly, the ordered porous structure of mesoporous silica provides a sheltered environment that enhance the stability of immobilized organic molecules to heat, extreme pH values, denaturants, and enzymatic digestion and thus beneficial for long-term remaining in force [33]. Lastly, mesoporous silica materials have good thermal stability, high mechanical robustness and favorable biocompatibility. Recently, a lot of such hybrid materials have been used for optical detection and separation of toxic metal ions [34–37]. However, most of them are operated in organic or in mixed aqueous-organic solvents [38–40]. Thus, the development of solid chemosensors with high selectivity and sensitivity for monitoring and absorbing Hg^{2+} in complex natural water samples remains a significant challenge.

Bearing this in mind, we synthesized a 1,8-naphthalimide-based receptor **P1** (Scheme 1) and immobilized it onto the channel surface of mesoporous silica (SBA-15) to develop new multifunctional nanomaterial SBA-**P1** used as chemosensor, adsorbent and toxicide

* Corresponding author. Tel.: +86 411 83702355; fax: +86 411 39893830.
E-mail address: cyduan@dlut.edu.cn (C. Duan).

0039-9140/$ – see front matter © 2010 Elsevier B.V. All rights reserved.
doi:10.1016/j.talanta.2010.12.008

Scheme 1 Synthesis procedure of SBA-P1

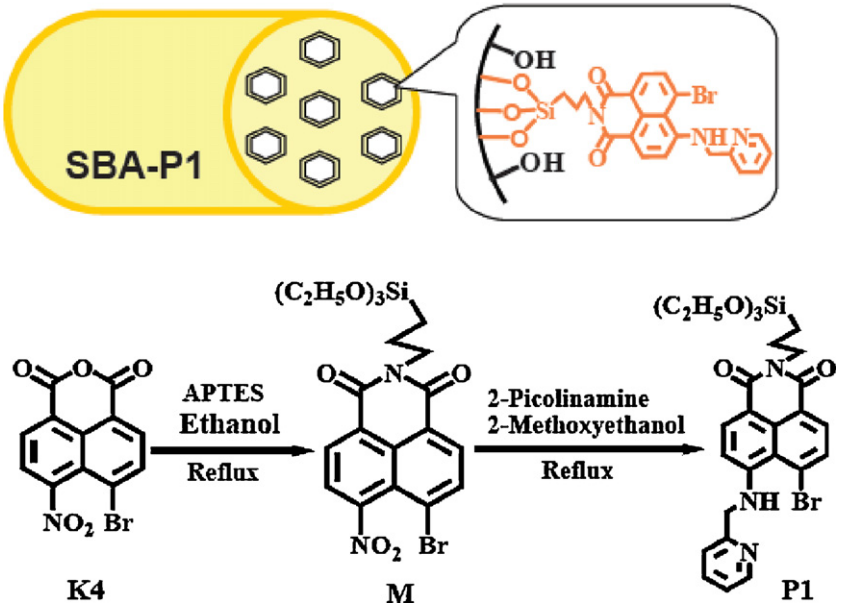

Scheme 1. Synthesis procedure of the SBA-**P1**.

responsible for Hg^{2+} with highly selective fluorescence changes and excellent adsorption.

2. Experimental

2.1. Reagents and instruments

All reagents and solvents were of analytical reagent (AR) grade and used without further purification unless otherwise noted. SBA-15 was procured from Jilin University High Technology Co. Ltd. (3-Aminopropyl)triethoxysilane, 2-(aminomethyl)pyridine were purchased from Aldrich. The metal salts employed were $LiClO_4$, $NaClO_4$, $KClO_4$, $Mg(ClO_4)_2$, $Cd(ClO_4)_2{\cdot}6H_2O$, $Mg(ClO_4)_2$, $Hg(ClO_4)_2{\cdot}3H_2O$, $Cr(ClO_4)_3{\cdot}6H_2O$, $Zn(ClO_4)_2{\cdot}6H_2O$, $AgClO_4{\cdot}H_2O$, $Co(ClO_4)_2{\cdot}6H_2O$, $Cu(ClO_4)_2{\cdot}6H_2O$ $Mn(ClO_4)_2{\cdot}6H_2O$, $Ni(ClO_4)_2{\cdot}6H_2O$, and $Pb(ClO_4)_2{\cdot}3H_2O$, respectively.

^1H NMR and ^{13}C NMR spectra were measured on a Varian INOVA 400M spectrometer with chemical shifts reported as ppm ($CDCl_3$, TMS as internal standard). ESI mass spectra were carried out on a HPLC-Q-TOF MS spectrometer using methanol as the mobile phase. X-ray powder diffraction (XRD) patterns of the SBA-15 and SBA-**P1** were recorded on a Rigaku D/max- 2000 X-ray powder diffractometer (Japan) using Cu Kα (l = 1.5405 Å) radiation. Transmission electron microscope (TEM) images were taken on a Hitachi H-9000 NAR transmission electron microscope under a working voltage of 300 kV. Fourier transform infrared spectroscopy (FT-IR) spectra were recorded on a Nicolet Magna-IR 750 spectrometer equipped with a Nic-Plan Microscope. UV–vis diffuses reflectance spectra were taken on a Shimadzu UV-2401PC spectrophotometer using $BaSO_4$ as the reference. Elemental analyses (C, H, N) were performed on an Elementar Vario EL analyzer. The nitrogen adsorption and desorption isotherms were measured at 77 K using an ASAP 2010 analyzer (Micromeritics Co. Ltd.). Surface areas were calculated by the Brunauer–Emmett–Teller (BET) method, and the pore volume and pore size distributions were calculated using the Barret–Joyner–Halenda (BJH) model. Fluorescence spectra of the solution were obtained using the FS920 spectrometer (Edinburgh Instruments). Both excitation and emission slit widths were 5 nm. The adsorption abilities of SBA-**P1** and SBA-15 for Hg^{2+} in water were measured by inductively coupled plasma spectrometer (Perkin Elmer). Fluorescence measurements were carried out in a 1 cm quartz cuvette with stirring the suspension of SBA-**P1**.

2.2. General procedures of spectra detection

Stock solution (2×10^{-2} M) of the aqueous perchlorate salts of Li^+, Na^+, K^+, Mg^{2+}, Ca^{2+}, Mn^{2+},Co^{2+}, Ni^{2+}, Cu^{2+}, Zn^{2+}, Cd^{2+}, Ag^+, Pb^{2+}, Cu^{2+} and Hg^{2+} were prepared. The suspension solutions of SBA-**P1** were prepared in pure water. Each time a 2 mL suspension of SBA-**P1** was filled in a quartz cell of 1 cm optical path length, and different stock solutions of cations were added into the quartz cell gradually by using a micro-pipette. The volume of cationic stock solution added was less than 100 μL with the purpose of keeping the total volume of testing solution without obvious change. All the spectroscopic measurements were performed at least in triplicate and averaged.

2.3. Synthesis of K4

Compound **K4** was synthesized according to the published procedures [41].

To a solution of acenaphthene (3.1 g, 20 mmol) in anhydrous DMF (10 mL) solution, n-bromosuccinimide (NBS) (3.6 g, 20.2 mmol) in anhydrous DMF (10 mL) was added dropwise in half an hour, the mixture was stirred for 4 h at room temperature. After the reaction was completed, the solvent was poured into water, yellow precipitates obtained were filtered off, washed with water and dried under vacuum. The crude product was then purified by chromatography on a silica gel column with petroleum ether to give 4-bromo-acenaphthene as a colorless crystal in 83% yield.

To a 100 mL flask, 4-bromo-acenaphthene (4.48 g, 19.3 mmol) was dissolved in glacial acetic acid (40 mL). The mixture solution of fuming nitric acid (4 mL) and glacial acetic acid (8 mL) was added dropwise in half an hour at 10–15 °C. The mixture was stirred for 10 h at room temperature, yellow precipitates obtained were filtered off. Crude product was purified by recrystallization from glacial acetic acid to give 1.9 g of 4-bromo-5-nitro-acenaphthene (yellow solid) in 36% yield.

To a 25 mL flask, $Na_2Cr_2O_7{\cdot}2H_2O$ (2.5 g, 8.4 mmol) was dissolved in glacial acetic acid (10 mL), then addition of 4-bromo-5-nitro-acenaphthene slowly, the mixture was heated to reflux for 3 h. After the reaction was completed, the solvent was poured into ice-water. After standing overnight, the resulting precipitate was filtered and washed with water until the filtrate becomes colorless. Crude product was purified by recrystallization from glacial acetic acid to give 1.9 g of **K4** (brown crystal) in 52% yield. ^{1}H NMR (DMSO, 400 MHz) δ 8.15 (d, 1H; Ar H), 8.36 (d, 1H; Ar H), 8.57 (d, 1H; Ar H), 8.78 (d, 1H; Ar H).

2.4. Synthesis of M

To a solution of **K4** (0.642 g, 2 mmol) in 50 mL anhydrous ethanol was added dropwise (3-aminopropyl) triethoxysilane (0.515 mL, 2.2 mmol) in 10 mL anhydrous ethanol. Under N_2, the mixture was then heated to reflux for 4 h. After the reaction was completed, the solvent was removed under reduced pressure. The crude product was then purified by chromatography on a silica gel column (CH_2Cl_2:EtOAc, 40:1, V/V) to give **M** as a pale solid in 85% yield. ^{1}H NMR ($CDCl_3$, 400 MHz) δ 0.758 (m, 2H), 1.212 (t, 9H), 1.634 (m, 2H), 3.812 (t, 6H), 4.163 (m, 2H), 7.925 (d, 1H), 8.211 (d, 1H), 8.512 (d, 1H), 8.704 (d, 1H). ^{13}C NMR ($CDCl_3$, 100 MHz). δ 7.756, 18.439, 21.650, 43.482, 58.618, 121.363, 122.745, 123.918, 124.149, 126.017,130.3, 132.416, 136.097, 151.446, 162.096, 162.885. HRMS (EI) calcd for $C_{21}H_{25}BrN_2O_7Si$, [M^++Na] 547.06, found 547.1.

2.5. Synthesis of P1

To a solution of **M** (104.8 mg, 2 mmol) in 50 mL anhydrous toluene was added dropwise 2-(aminomethyl)pyridine (0.3 mL) in 10 mL anhydrous toluene. Under N_2, the mixture was then heated to reflux for 10 h. After the reaction was completed, the solvent was removed under reduced pressure. The crude product was then purified by chromatography on a silica gel column (CH_2Cl_2:EtOAc, 20:1, V/V) to give **P1** as a orange solid in 87.8 mg in 75% yield. ^{1}H NMR ($CDCl_3$, 400 MHz) δ 0.740 (m, 2H), 1.230 (m, 9H), 1.44 (m, 2H), 3.810 (m, 2H), 4.116 (m, 2H) 4.703 (t, 2H), 4.737 (s, 2H), 6.787 (d, 1H), 7.271 (t, 1H), 7.376 (d, 1H), 7.529 (s, N-H), 7.735 (t, 1H), 7.844 (d, 1H), 8.313 (d, 1H), 8.450 (d, 1H), 8.671 (d, 1H), 8.927 (d, 1H). ^{13}C NMR ($CDCl_3$, 100 MHz). δ 8.17, 18.9, 21.60, 30.3, 42.91, 49.39, 58.54, 106.70, 110.45, 118.34, 122.51, 125.05, 126.64, 129.00, 131.19, 132.41, 135.04, 137.16, 149.67, 155.42, 163.99, 167.88. HRMS (EI) calcd for $C_{27}H_{32}BrN_3O_3Si$, [M^++H] 586.13, found 586.2.

2.6. Synthesis of hybrid material SBA-P1

P1 (0.234 g, 0.4 mmol) and SBA-15 (1.0 g) are dissolved in anhydrous toluene (50 mL) and stirred in reflux condition under N_2 for 24 h. Then, the precipitate was filtered, and washed several times with toluene and CH_2Cl_2 to rinse away any surplus **P1**, a yellow power was obtained and denoted as SBA-**P1**, like the literature method for the preparation of SBA-**P2** [42]. Elemental analysis, found: N, 0.37, C, 3.94, H 1.82.

2.7. Adsorption ability of SBA-P1 for Hg^{2+}

SBA-**P1** (10 mg) and SBA-15 (10 mg) were added to 50 mL of the Hg^{2+} solution (about 0.1 μg mL^{-1}), respectively. The mixture was stirred for 1 h. After filtration, the concentration of residual Hg^{2+} in the filtrate was analyzed by inductively coupled plasma source mass spectrometer (ICP).

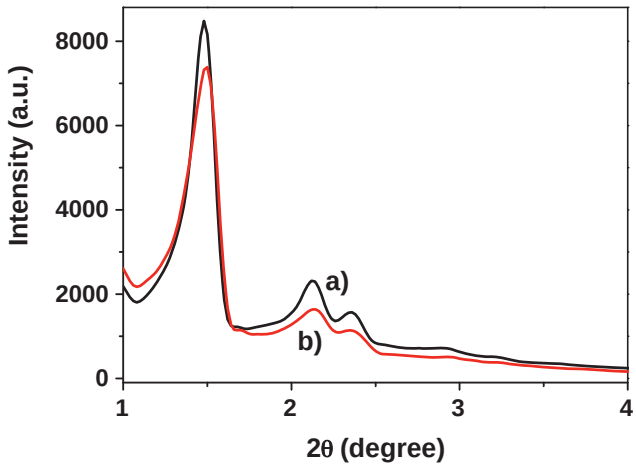

Fig. 1. XRD patterns of (a) SBA-15 and (b) SBA-**P1**.

3. Results and discussion

3.1. Synthesis and characterization of SBA-P1

Compounds **K4** was prepared according to the reported procedures. **P1** was easily synthesized by conjugating 2-(aminomethyl) pyridine and **M**. **P1** was covalently attached onto SBA-15 by sol–gel reaction in anhydrous toluene (Scheme 1). The functionalized silica nanomaterial was well characterized EA and XRD as well as several spectroscopic methods.

Fig. 1 shows the low-angle XRD patterns of SBA-15 and SBA-**P1**. All the curves exhibit three characteristic diffraction peaks that can be indexed to (1 0 0), (1 1 0), and (2 0 0) diffraction associated with typical two-dimensional hexagonal symmetry (*P6*mm). The results indicated that the long-range hexagonal symmetry of SBA-15 was preserved after the sequence modification of fluorescence dye **P1**. However, the intensities of these characteristic diffraction peaks decreased slightly after grafting of **P1** with respect to SBA-15. This may be attributed to a reduction in the X-ray scattering contrast between the silica walls and pore-filling material [43]. The TEM images of the SBA-**P1** exhibited highly ordered hexagonal arrays of mesopores with one-dimensional channels (Fig. 2) throughout the sample, indicating that the channel structure of SBA-15 is not destroyed by incorporation of **P1** receptor.

To further investigate porosity changes of the mesoporous silica by introduction of **P1**. The low-temperature N_2 adsorption–desorption isotherms was characterized. As shown in Fig. 3, the isotherms of SBA-15 and SBA-**P1** were of type IV as defined by IUPAC, characteristic of mesoporous solids. The volume adsorbed for all isotherms increased sharply at a relative pressure (P/P_0) of approximately 0.75, representing a capillary condensation of nitrogen within the uniform mesopore structure. The inflection position shifted slightly toward lower relative pressures and the volume of nitrogen adsorbed decreased with functionalization, which was indicative of a reduction in pore size. As expected, the Brunauer–Emmett–Teller (BET) surface area of SBA-**P1** sample declined from 571 m^2/g to 445 m^2/g due to the linkage of **P1**. Likewise, the pore volume shrinked to 0.605 cm^3/g from 0.912 cm^3/g for the parent materials. Furthermore, the Barret–Joyner–Halenda (BJH) pore diameters distribution of SBA-**P1** showed a decrease in diameter by 2.0 nm compared with that of SBA-15 (Fig. 3) [44]. These results indicated that the mesoporous structure of SBA-15 was maintained after attachment of the functional unit [45]. Furthermore, from the result of elemental analysis (EA), we noted that the SBA-**P1** consisted of only about 8.0 wt% of **P1**. That is to say, 20 ppm **P1**-modified silica nanomaterial used

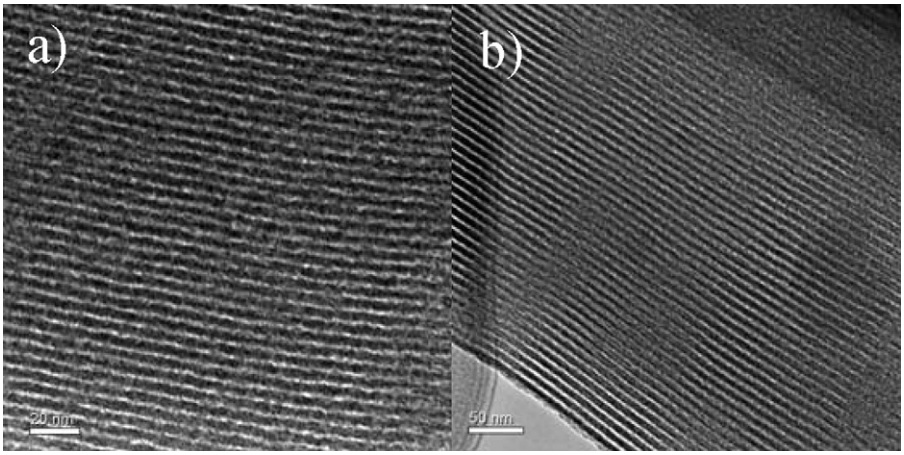

Fig. 2. TEM images of (a) SBA-15 and (b) SBA-**P1**.

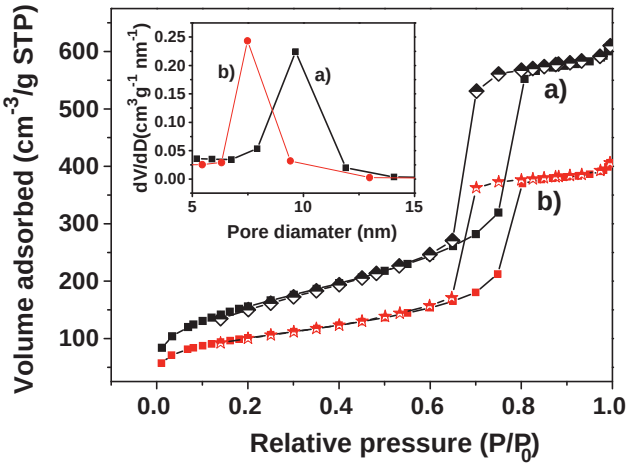

Fig. 3. Nitrogen adsorption–desorption isotherms of (a) SBA-15 and (b) SBA-**P1**. (b) Inset: corresponding pore size distribution for (a) SBA-15 and (b) SBA-**P1**.

in our experiments corresponded to about 3 μM of receptor **P1**.

Fig. 4(a) depicts the corresponding UV–vis diffuse reflectance spectra of SBA-15 and SBA-**P1**. As can be seen, a broad adsorption band centered at about 450 nm emerged for SBA-**P1**, implying the successful incorporation of compound **P1** onto SBA-15. These bands could be attributed to the typical electronic transition of the aromatic ring [46]. For further structural proof of the SBA-**P1**, we carried out FT-IR spectroscopy of both SBA-15 and SBA-**P1**. Fig. 4(b) depicts the FT-IR spectra of SBA-15 and SBA-**P1**, respectively. The bands at about 3430 cm^{-1} and 1635 cm^{-1} were attributed to the stretching (3430 cm^{-1}) and bending (1635 cm^{-1}) vibrations of the surface silanol groups and the remaining adsorbed water molecules [47], and a strong band centered at 1100 cm^{-1} was attributed to the stretching vibration of siloxane (–Si–O–Si–) groups. After the modification, SBA-**P1** material showed characteristic bands for aliphatic C–H stretching vibrations at around 2925 cm^{-1} and C=C stretching vibrations at about 1367 cm^{-1}. Accordingly, these observations indicated the bonding between the fluorescent chromophore (**P1**) and surface SiO–H groups on SBA-15.

3.2. The application of SBA-P1 as chemosensor and absorbent for Hg^{2+} in water

The binding behavior of SBA-**P1** toward different cations (Hg^{2+}, Cu^{2+}, Zn^{2+}, Cd^{2+}, Pb^{2+}, Cr^{3+}, Mn^{2+}, Ni^{2+}, Co^{2+}, Ag^{+}, Mg^{2+}, Ca^{2+}, Li^{+}, Na^{+}, K^{+}) was investigated by fluorescence spectroscopy. The fluorescence intensities were recorded at 480 nm within 2 min after the addition of these metal ions (1×10^{-4} mol L^{-1}) in suspension of SBA-**P1** (20 μg mL^{-1}). Fig. 5, illustrated the fluorescence responses of SBA-**P1** to various metal ions and its selectivity for Hg^{2+}. No significant spectral changes of the suspension solution occurred in the presence of alkali or alkaline earth metals and the first-row transition metals, such as, Cu^{2+}, Zn^{2+}, Cd^{2+}, Pb^{2+}, Mn^{2+}, Ni^{2+}, Co^{2+}, Ag^{+}, Cr^{3+}, and Mg^{2+}, Ca^{2+}, Li^{+}, Na^{+}, K^{+}, while the addition of Hg^{2+} ions into the suspension of SBA-**P1** produced a dramatic decrease in fluorescence intensity. Adding 1 equiv. of Hg^{2+} to the above suspension gave rise to drastic quenching of their fluorescence intensities,

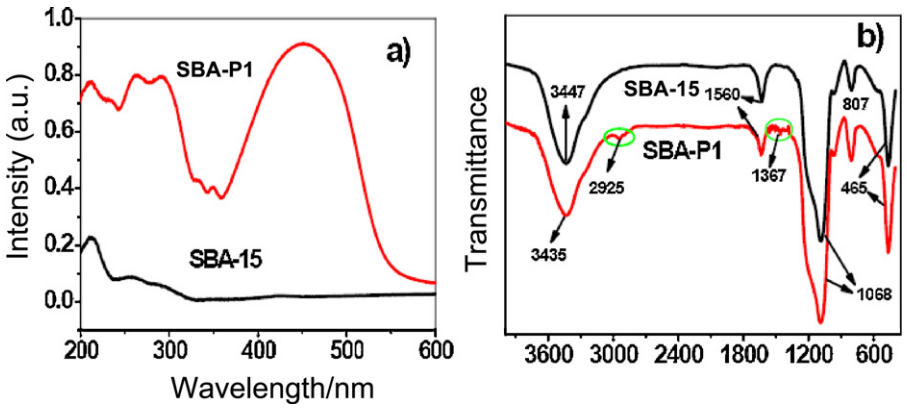

Fig. 4. (a) UV–vis diffuses reflectance spectra of SBA-15 and SBA-**P1**. (b) FT-IR spectra of SBA-15 and SBA-**P1**.

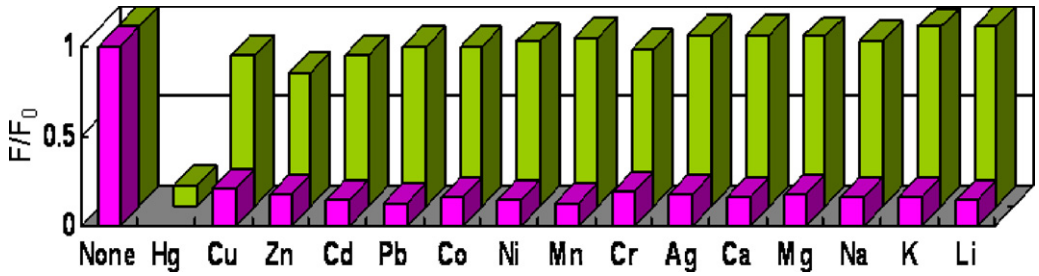

Fig. 5. Normalized fluorescence responses of SBA-**P1** (20 μg mL^{-1}) to various cations in water. The green bars represent the emission intensities of SBA-**P1** in the presence of cations of interest (all are 1×10^{-4} mol L^{-1}). The red bars represent the change of the emission that occurs upon the subsequent addition of 1×10^{-4} mol L^{-1} of Hg^{2+} to the above solution. The intensities were recorded at 480 nm, excitation at 447 nm. (For interpretation of the references to color in this figure legend, the reader is referred to the web version of the article.)

revealing that Hg^{2+} could have specific effects on the luminescence spectra, and the Hg^{2+}-specfic responses were not disturbed by the competitive ions (Fig. 5).

The complexation of Hg^{2+} by SBA-**P1** was also investigated by means of fluorescence titration. The titration was performed using 20 μg mL^{-1} suspension of SBA-**P1** (pH = 7.0). A about 14-fold quenching of fluorescence and a continuous red shift of the emission peak from 480 to 491 nm were observed upon the addition of 1.5×10^{-4} mol L^{-1} of Hg^{2+} compared to that of free SBA-**P1** (Fig. 6), which could be explained in terms of the prevention of the excited-state ICT process from the donor to the acceptor. The fluorescence quenching of naphthalimide moiety by Hg^{2+} ion could be ascribed to a PET (photo-induced energy transfer) mechanism induced by the chelation of Hg^{2+} with the amine and the nitrogen atom of pyridine group [48]. Fluorescence titration profile at 480 nm versus 1.5×10^{-4} mol L^{-1} of Hg^{2+} in the suspension of SBA-**P1** was shown in Fig. 6 inset. The detection limit for Hg^{2+} in water was established at 0.2 μg mL^{-1} under current experimental conditions.

Fluorophores are usually disturbed by the proton in the detection of metal ions, so their low sensitivities to the operational pH value are extremely expected. For practical applicability, the proper pH condition of this new hybrid material was also evaluated. The fluorescence emission intensities of SBA-**P1** with and without Hg^{2+} as a function of pH were shown in Fig. 7. The pH-controlled emission measurements revealed that SBA-**P1** could respond to Hg^{2+} in the pH range from 4.0 to 11.0 without obvious fluorescent intensity changes. This result suggested that no buffer solutions were required for the detection of Hg^{2+}, which was convenient for practical application.

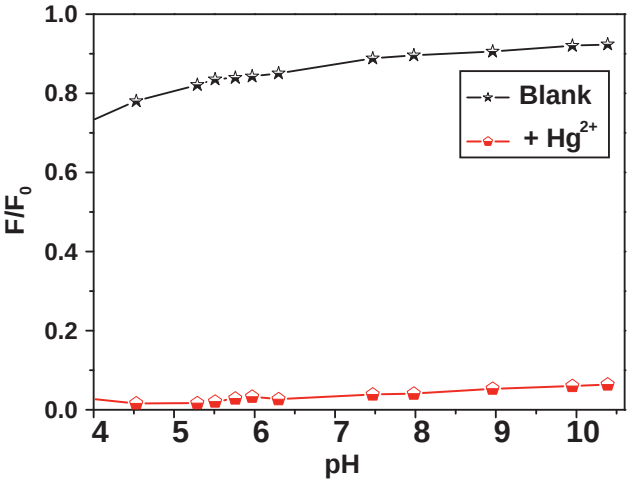

Fig. 7. Variations of fluorescence intensity at 480 nm of SBA-**P1** (20 μg mL^{-1}) in aqueous solution with (bottom) and without (up) Hg^{2+} ion (1×10^{-4} mol L^{-1}) as a function of pH. Excitation at 447 nm.

Reversibility and regeneration are also important factors for the development of devices for sensing analytes in practical applications. We examined the recovery of the 1,8-naphthalimide-based functional material after bonding Hg^{2+}. The hybrid material SBA-**P1** was treated with EDTA and base, and the quenching fluorescence intensity upon exposure to Hg^{2+} was almost reversible (Fig. 8). This result clearly indicated that the 1,8-naphthalimide-based hybrid material was stable in operating conditions, and demonstrated the

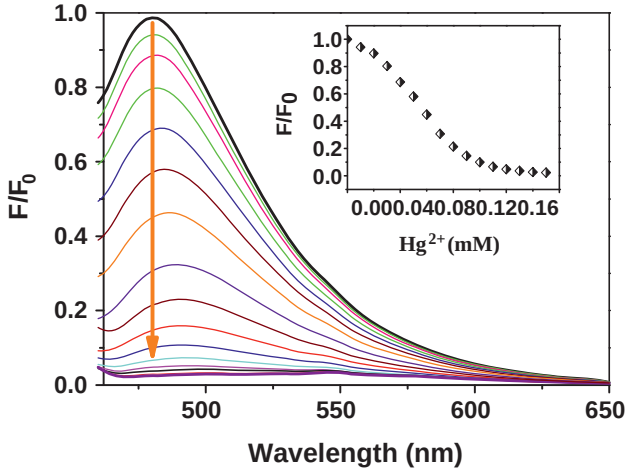

Fig. 6. Fluorescence spectra of SBA-**P1** (20 μg mL^{-1}) upon the addition of various amounts of Hg^{2+} (0–1.5×10^{-4} mol L^{-1}) in water (pH = 7). The inset exhibits a fluorescence titration profile at 480 nm upon the addition of Hg^{2+} (excitation at 447 nm).

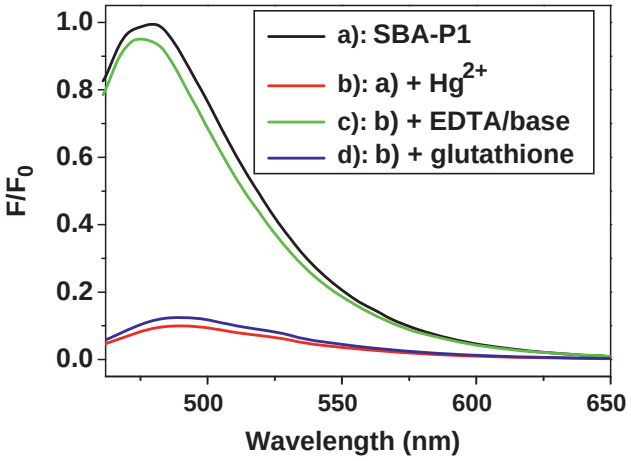

Fig. 8. Fluorescent spectra of SBA-**P1** (20 μg mL^{-1}) in water (a) without and (b) with Hg^{2+}, and (c) after treatment with EDTA/base (5 equiv. of Hg^{2+}) in (b) solution, (d) treatment with glutathione (10 equiv. of Hg^{2+}) in (b) solution. Excitation at 447 nm.

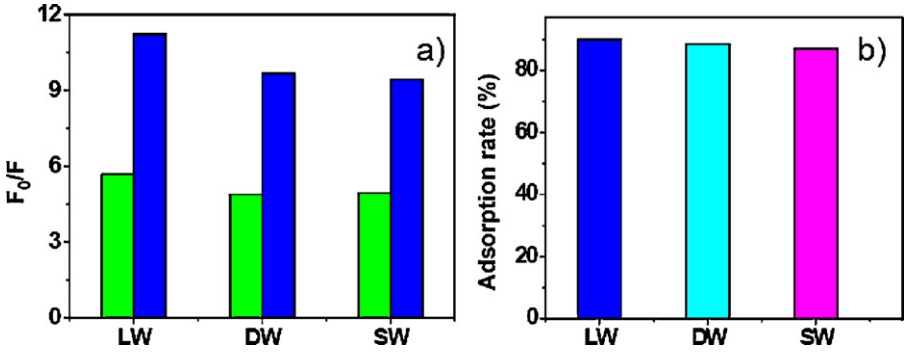

Fig. 9. The performance of SBA-**P1** to Hg^{2+} in practical water samples. (a) Sensitivity of SBA-**P1** to Hg^{2+} in different water samples: laboratory pure water (LW), drinking water (DW) and seawater (SW). The green and blue bars represent the emission intensities of SBA-**P1** in the presence of 5×10^{-5} mol L^{-1} (green bars) and 1×10^{-4} mol L^{-1} (blue bars) of Hg^{2+}, respectively. (b) Absorption capability of SBA-**P1** to Hg^{2+} in complex natural samples. (For interpretation of the references to color in this figure legend, the reader is referred to the web version of the article.)

recyclable of SBA-**P1** in the potential biological and environmental usage.

The mesoporous silica material features excellent biocompatibility, which enables such silica-based materials to become the promising substrates in biomedical and biotechnological applications, such as cell-type recognition, disease diagnosis, intracellular imaging, and drug/gene delivery [49,50]. Mercury has been known to be a toxic and dangerous element to human beings when ingested or inhaled. And exposure of the human body to even a low concentration of Hg^{2+} can lead to neurological diseases and other organs damage [51]. Traditionally, glutathione is one of the common effective toxicide for mercury poisoning. However, one disadvantage of this toxicide is that an enzymatic digestion effect will take place and the metal ions may be released again [52]. As for SBA-**P1**, the coordination ability was much stronger than that of glutathione (Fig. 8(d)). Moreover, the embedded effective functional groups were expected to be stable against enzymatic digestion due to the protection of the mesopores and thus a long-acting toxicide. In particular, the silica material can be eliminated from the body by metabolism process after adsorbing Hg^{2+}. To sum up, we believe SBA-**P1** is a promising multifunctional material which can be used in biological field.

As for a practical environmental cleanup of the hybrid material, the adsorption ability of SBA-**P1** for Hg^{2+} in solid–liquid phase was also estimated. The concentration of Hg^{2+} solution before and after treating with SBA-**P1** was estimated by inductively coupled plasma source mass spectrometer (ICP) [33]. It is well known that the inner surface of SBA-15 covered with abundant hydroxyl groups on the pore walls, SBA-15 could adsorb Hg^{2+} (17%) from the ICP analytical measurements. However, above 90% of Hg^{2+} was adsorbed by SBA-**P1** due to incorporation of a Hg^{2+} receptor (**P1**) onto SBA-15. Moreover, the XRD patterns of Hg^{2+}-loaded SBA-**P1** were mostly similar with the parent materials, implying upstanding stability of this hybrid material. These results suggested that the functional material had potential environmental applications, such as optical sensing and removal of toxic metal ions in industrial waste water.

In order to show the feasibility of the hybrid material as chemosensor and absorbent for Hg^{2+} in potential practical applications, we studied the performance of SBA-**P1** in natural water samples. The addition of 5×10^{-5} mol L^{-1} (green bars) and 1×10^{-4} mol L^{-1} (blue bars) of Hg^{2+} to the SBA-**P1** suspension dispersed in laboratory pure water (LW) affords about 5.5-fold and 11-fold quenching of fluorescence intensity, respectively. Then we tested the responding ability of SBA-**P1** to Hg^{2+} dispersed in natural water. Water samples were collected from two significantly different sources: some drinking water (DW) from Dalian City (Liaoning Province, China) and seawater (SW) from the Yellow Sea (Dalian, area of China). The Hg^{2+}-induced fluorescence quenching was not significantly affected in the presence of different water source (Fig. 9(a)). We also studied the influence of water source to the absorption capability of SBA-**P1** for Hg^{2+} by ICP. As shown in Fig. 9(b), no significant difference was found. The preliminary investigations in natural water samples including seawater and drinking water indicate that SBA-**P1** features an excellent Hg^{2+} chemosensor and adsorbent to environmentally relevant mercury in complex natural samples.

4. Conclusions

In conclusion, a novel hybrid material (SBA-**P1**) has been designed by covalent coupling of 1,8-naphthalimide-based receptor **P1** within the channels of mesoporous material SBA-15. The functionalized silica nanomaterial recognized and absorbed Hg^{2+} with a high degree of selectivity among heavy metal ions in natural aqueous solution. The novel solid fluorescent chemosensor is reversible for Hg^{2+} and can be used in a wide pH span. We believe the combination of well-defined hybrid materials and organic receptors can play a pivotal role in the development of a new generation of toxic metal ions absorbent and toxicide.

References

[1] D.W. Boening, Chemosphere 40 (2000) 1335–1351.
[2] H.H. Harris, I. Pickering, G.N. George, Science 301 (2003) 1203.
[3] T.W. Clarkson, L. Magos, G.J.N. Myers, Engl. J. Med. 349 (2003) 1731–1735.
[4] C.M.L. Carvalho, E.-H. Chew, S.I. Hashemy, J. Lu, A. Holmgren, J. Biol. Chem. 283 (2008) 11913–11916.
[5] G. Guzzi, C.A.M. La Porta, Toxicology 244 (2008) 1–12.
[6] X. Chen, S.W. Nam, M.J. Jou, Y. Kim, S.J. Kim, S. Park, J. Yoon, Org. Lett. 11 (2009) 5235–5238.
[7] J. Huang, Y. Xu, X. Qian, J. Org. Chem. 74 (2009) 2167–2170.
[8] G.J. He, Y.G. Zhao, C. He, Y. Liu, C.Y. Duan, Inorg. Chem. 47 (2008) 5169–5176.
[9] X.L. Zhang, Y. Xiao, X.H. Qian, Angew. Chem. Int. Ed. 47 (2008) 8025–8032.
[10] F. Song, S. Watanabe, P.E. Floreancig, Kazunori Koide, J. Am. Chem. Soc. 130 (2008) 16460–16461.
[11] X. He, Y. Wang, K. Ling, Talanta 72 (2007) 747–754.
[12] G.J. He, D. Guo, C. He, X.L. Zhang, X.W. Zhao, C.Y. Duan, Angew. Chem. Int. Ed. 48 (2009) 6132–6135.
[13] Y.G. Zhao, Z.H. Lin, C. He, H.M. Wu, C.Y. Duan, Inorg. Chem. 45 (2006) 10013–10015.
[14] Z. Wang, D.Q. Zhang, D.B. Zhu, Anal. Chim. Acta 549 (2005) 10–13.
[15] X. Zhu, S. Fu, W.K. Wong, J. Guo, W.Y. Wong, Angew. Chem. Int. Ed. 45 (2006) 3150–3154.
[16] C. Huang, Z. Yang, K. Lee, H. Chang, Angew. Chem. Int. Ed. 46 (2007) 6824–6828.
[17] K. Feng, F. Hsu, K. Bota, X.R. Bu, Microchem. J. 81 (2005) 23–27.
[18] S. Yoon, E.W. Miller, Q. He, P.H. Do, C.J. Chang, Angew. Chem. Int. Ed. 46 (2007) 6658–6661.
[19] E.M. Nolan, S.J. Lippard, J. Am. Chem. Soc. 129 (2007) 5910–5918.
[20] J. Lee, M.S. Han, C.A. Mirkin, Angew. Chem. Int. Ed. 46 (2007) 4093–4096.
[21] S.V. Wegner, A. Okesli, P. Chen, C. He, J. Am. Chem. Soc. 129 (2007) 3474–3475.
[22] X.J. Xue, F. Wang, X.G. Liu, J. Am. Chem. Soc. 130 (2008) 3244–3245.
[23] A.E. Kadib, R. Chimenton, A. Sachse, F. Fajula, A. Galarneau, B. Coq, Angew. Chem. Int. Ed. 48 (2009) 4969–4972.

[24] L. Mu, W. Shi, G. She, J.C. Chang, S. Lee, Angew. Chem. Int. Ed. 48 (2009) 3469–3472.
[25] I. Cesarino, G. Marino, J.D.R. Matos, É.T.G. Cavalheiro, Talanta 75 (2008) 15–21.
[26] D.P. Ferris, Y. Zhao, N.M. Khashab, H.A. Khatib, J.F. Stoddart, E.I. Zink, J. Am. Chem. Soc. 131 (2009) 1686–1688.
[27] G. Zhang, G. Zhang, J.H. Chua, R. Chee, E.H. Wong, A. Agarwal, K.D. Buddharaju, N. Singh, Z. Gao, N. Balasubramanian, Nano Lett. 8 (2008) 1066–1070.
[28] F. Gao, F. Luo, X. Chen, W. Yao, J. Yin, Z. Yao, L. Wang, Talanta 80 (2009) 202–204.
[29] C.F. Jones, D.W. Grainger, Adv. Drug Deliv. Rev. 61 (2009) 438–456.
[30] S. Hartono, S.Z. Qiao, K. Jack, B.P. Ladewig, Z. Hao, G.Q. Lu, Langmuir 25 (2009) 6413–6424.
[31] A.P. Wight, M.E. Davis, Chem. Rev. 102 (2002) 3589–3614.
[32] L. Basabe-Desmonts, D.N. Reinhoudt, M. Crego-Calama, Chem. Soc. Rev. 36 (2007) 993–1017.
[33] S. Hudson, J. Cooney, E. Magner, Angew. Chem. Int. Ed. 47 (2008) 8582–8594.
[34] P. Zhou, Q.T. Meng, G.J. He, H.M. Wu, C.Y. Duan, X. Quan, J. Environ. Monit. 11 (2009) 648–653.
[35] Y. Jiang, Q. Gao, H. Yu, Y. Chen, F. Deng, Micropor. Mesopor. Mater. 103 (2007) 316–324.
[36] A.M. Burkea, J.P. Hanrahana, D.A. Healy, J.R. Sodeau, J.D. Holmes, M.A. Morrisa, J. Hazard. Mater. 164 (2009) 229–234.
[37] S.J. Lee, J.-E. Lee, J. Seo, Y. Jeong, S.S. Lee, J.H. Jung, Adv. Funct. Mater. 17 (2007) 3441–3446.
[38] H.J. Kim, S.J. Lee, S.Y. Park, J.H. Jung, J.S. Kim, Adv. Mater. 20 (2008) 3229–3234.
[39] S.J. Lee, S.S. Lee, M.S. Lah, J.M. Hong, J.H. Jung, Chem. Commun. (2006) 4539–4541.
[40] S.J. Lee, S.S. Lee, J.Y. Lee, J.H. Jung, Chem. Mater. 18 (2006) 4713–4715.
[41] A.T. Peters, Y.S.S Behesti, J. Soc. Dyers. Colour (1989) 29–35.
[42] Q.T. Meng, X.L. Zhang, C. He, G.J. He, P. Zhou, C.Y. Duan, Adv. Funct. Mater. 20 (2010) 1903–1909.
[43] D. Peĭrez-Quintanilla, I. Hierro, M. Fajardo, I. Sierra, J. Mater. Chem. 16 (2006) 1757–1764.
[44] C.X. Song, X.L. Zhang, C.Y. Jia, P. Zhou, X. Quan, C.Y. Duan, Talanta 81 (2010) 643–649.
[45] J. Wang, L. Huang, M. Xue, Y. Wang, L. Gao, J.H. Zhu, Z. Zou, J. Phys. Chem. C 112 (2008) 5014–5022.
[46] L. Gao, Y. Wang, J. Wang, L. Huang, L. Shi, X. Fan, Z. Zou, T. Yu, M. Zhu, Z. Li, Inorg. Chem. 45 (2006) 6844–6850.
[47] L. Li, H. Sun, C. Fang, J. Xu, J. Jin, C. Yan, J. Mater. Chem. 17 (2007) 4492–4498.
[48] E.M. Nolan, M.E. Racine, S.J. Lippard, Inorg. Chem. 45 (2006) 2742–2749.
[49] M. Vallet-Regí, F. Balas, D. Arcos, Angew. Chem. Int. Ed. 46 (2007) 7548–7558.
[50] I.I. Slowing, B.G. Trewyn, S. Giri, V.S.-Y. Lin, Adv. Funct. Mater. 17 (2007) 1225–1236.
[51] E.M. Nolan, S.J. Lippard, Chem. Rev. 108 (2008) 3443–3480.
[52] K.M.L. Taylor-Pashow, J.D. Rocca, Z. Xie, S. Tran, W. Lin, J. Am. Chem. Soc. 131 (2009) 14261–14263.